

Bearing capacity of spatially variable unsaturated fly ash deposit using random field theory

Abhijit Anand and Rajib Sarkar*

Department of Civil Engineering, Indian Institute of Technology (Indian School of Mines) Dhanbad, Dhanbad 826 004, India

The aim of the present study is to examine the bearing capacity of a spatially variable, unsaturated fly ash deposit, based on finite element limit analyses. Strength nonlinearity of fly ash, arising due to partial saturation, has been modelled based on the well-known van Genuchten (vG) fitting parameters, obtained from the water retention characteristics curve (WRCC). For the probabilistic study, WRCC fitting parameters and angle of internal friction of the fly ash deposit have been considered as stationary Gaussian random fields within a practicable range of coefficient of variation and anisotropic correlation lengths. Random field has been generated based on the Karhunen–Loeve expansion method. Adequate numbers of Monte-Carlo simulations have been executed to evaluate the probabilistic distribution of the bearing capacity, considering strength nonlinearity as well as the random distribution of the input parameters. Influence of stationary spatial variation of WRCC fitting parameters and friction angle on the probability of failure of a footing resting on the fly ash deposit is presented and observations are duly explained. The results of this study would be useful for practising engineers to design a safe fly ash fill and therefore offer a sustainable solution for the bulk utilization of fly ash in geotechnical engineering applications.

Keywords: Bearing capacity, finite element limit analysis, geotechnical engineering applications, probabilistic analysis, strength nonlinearity, unsaturated fly ash.

AN efficient and sustainable solution for disposal of bulk volume of fly ash generated by thermal power plants has become a challenging task for engineers in the last few decades. Fly ash is an industrial waste produced by coal-based thermal power plants and contains predominantly the fused residues of clay minerals present in the coal. Fly ash, if not utilized or disposed of properly, may cause serious environmental hazards^{1,2}. In recent years, several researchers have established the efficacy of fly ash as an alternative and sustainable geomaterial for the construction of embankments, filling of low-lying areas, reclamation of unused sites, etc.^{1,3–5}. Moreover, in 2015 alone,

coal-based energy sources supplied 29% of the energy globally. Despite the increase in the use of renewable energy sources, coal is anticipated to remain the chief source of energy till 2035, with a total global energy share of 24% (ref. 6). Consequently, a large volume of unutilized fly ash would be generated and therefore, bulk utilization of fly ash in geotechnical engineering applications may provide a promising solution for its bulk disposal.

Bearing capacity is the key design parameter to be considered while establishing the suitability of fly ash in geotechnical engineering applications, as an alternative to natural soil. Majority of the surface or near-surface soils on earth are partially saturated owing to various variable environmental and geo-hydrological conditions. Under partially saturated state, the strength of a geomaterial is substantially affected due to negative pressure (suction) arising due to the presence of a contractile skin and the capillary action of water⁷. The relative proportion and distribution of pore-air and pore-water pressure plays a vital role in altering the intergranular contact stresses between the particles within the soil matrix. Fredlund and Morgenstern⁷ have attempted to model the mechanical behaviour of partially saturated soil by introducing two independent stress state variables, i.e. net normal stress ($\sigma - u_a$) and matric suction ($u_a - u_w = \psi$), where σ is the normal stress, u_a the pore-air pressure, u_w the pore-water pressure and ψ is the matric suction. The shear strength constitutive equation for an unsaturated soil, therefore, may be modified in terms of two independent stress state variables as⁸

$$\tau_f = c' + (\sigma_f - u_a)_f \tan \phi' + (u_a - u_w)_f \tan \phi_b, \quad (1)$$

where τ_f is the shear strength, c' the true effective cohesion, σ_f the normal stress, $(\sigma_f - u_a)_f$ the net normal stress on the failure plane at failure, $(u_a - u_w)_f$ the matric suction at failure, ϕ' the effective friction angle and ϕ_b is the suction angle representing the variation of shear strength with matric suction.

Furthermore, several researchers have addressed the problem of bearing capacity of shallow strip footing by introducing two independent stress state concepts^{9–11}.

*For correspondence. (e-mail: rajib@iitism.ac.in)

With subsequent advances in research, the inherent limitation of independent stress variable concepts has been reported as it failed to satisfactorily predict the mechanical behaviour of unsaturated soil for suction value higher than its air-entry value (AEV)¹². To account for the strength nonlinearity of the geomaterials with matric suction, Vanapalli and Mohamed¹³ incorporated water retention characteristics curve (WRCC) parameters into the bearing capacity equation. Substantial effort has been made by researchers to study the influence of matric suction on the bearing capacity of a shallow strip foundation based on various empirical and semi-empirical approaches^{12–17}. Vahedifard and Robinson¹² developed a closed-form method to estimate the bearing capacity of shallow strip footing overlying an unsaturated soil deposit by adopting the van Genuchten¹⁸ WRCC fitting parameters based on a ‘total cohesion’ concept. Oh and Vanapalli¹⁹ obtained the pressure–settlement relation of an unsaturated cohesive soil by extending the total stress approach and using modified engineering parameters based on WRCC.

Conventionally, WRCC is obtained by fitting a prescribed parametric model to the limited number of test data available²⁰. The limited number of test data and model selection uncertainty make the evaluation of WRCC fitting parameters a challenging task. Therefore, a deterministic estimation of WRCC fitting parameters with sufficient reliability is difficult. Furthermore, an accurate determination of WRCC parameters is restrained due to inherent inadequacy of instruments to measure a large range of matric suction. Measurement of a large set of data to enhance the accuracy increases the cost as well as duration of the project. Due to the aforementioned limitations, accurate determination of WRCC parameters of a geomaterial is seldom possible. Furthermore, deterministic analyses based on a single set of WRCC parameters are highly questionable. In addition, when fly ash is used in geotechnical engineering applications as a structural fill, accurate determination of its engineering parameters is vital while designing a shallow foundation over such a deposit. Engineering properties of fly ash are highly uncertain in nature and depend on several factors such as boiler condition, quality of coal, source of collection of the fly ash sample, etc. Therefore, bearing capacity analysis of shallow foundation over an unsaturated fly ash deposit based on deterministic framework may not yield a reliable solution. The properties of the fly ash may also vary spatially due to improper compaction and poor control over placement of the fly ash fill. Recently, several researchers have shown growing interest in performing a random field theory analysis by assuming spatially varying environmental and hydrological properties²¹ as well as varying fluctuation in the groundwater table depth²².

In view of the aforementioned gaps, the present study focuses on the inherent variability of an unsaturated fly ash deposit on the overall reliability of the bearing capacity of a shallow strip footing. Relative significance of spatial

correlation lengths and coefficient of variation of van Genuchten¹⁸ WRCC fitting parameters and angle of internal friction, on the statistical distribution of bearing capacity has been highlighted. For this, the present study considers nonlinear finite element limit analyses (FELA) with random field theory using Monte-Carlo simulation (MCS). For a comparative study and to establish the significance of some of the critical parameters, deterministic analyses have also been carried out.

Methodology

Quantification of suction stress-based engineering parameters

Under partial saturation of the soil matrix, due to the complex stress transfer mechanism between the contractile skin (air–water interface), an additional stress state is developed. Consequently, the shear strength of the soil changes with change in its stress state owing to variation in the degree of saturation of the soil–pore matrix. To quantify the change in shear strength of the soil with matric suction, several researchers extended the prominent Mohr–Coulomb (M–C) failure theory to incorporate suction stress into the analysis. Conventionally, the relationship between shear strength and matric suction of a geomaterial is linear up to AEV. With further increase in matric suction within the transition zone and residual zone, shear strength varies nonlinearly with matric suction. Figure 1 shows the typical variation of shear strength with matric suction for a geomaterial. Consequently, based on several laboratory investigations, it was found that there exists a direct correspondence between the strength nonlinearity of the soil and its inherent WRCC. Figure 1 depicts the three major broad regions of WRCC and its consequent role on the shear strength envelope for a typical soil material. To comprehensively describe the shear strength behaviour of an unsaturated geomaterial for the entire range of suction, the M–C equation is extended by incorporating WRCC parameters into it.

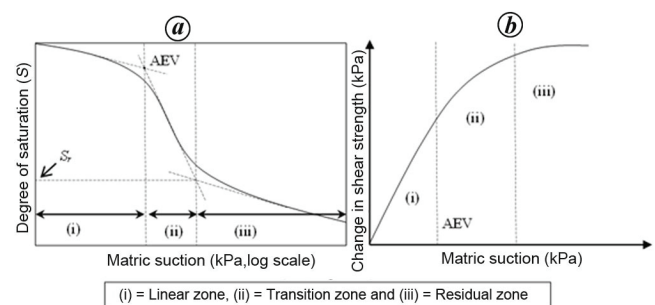


Figure 1. Typical relationship between shear strength and matric suction of a geomaterial: (a) water retention characteristic curve and (b) strength envelope.

Under partially saturated state, Lu *et al.*²³ extended the effective stress expression of Bishop²⁴ as

$$\sigma' = (\sigma - u_a) + \chi(u_a - u_w), \tag{2}$$

$$\sigma' = (\sigma - u_a) - \sigma_s, \tag{3}$$

$$\sigma' = (\sigma - u_a) + [S_e(u_a - u_w)], \tag{4}$$

where σ' is the effective stress, u_a and u_w are pore-air and pore-water pressure respectively, $(u_a - u_w) = \psi$ the matric suction, χ the Bishop's effective stress parameter (0 for dry and 1 for saturated soil), $\sigma_s = -\chi(u_a - u_w)$ is the suction stress and S_e is the effective degree of saturation defined as

$$S_e = \frac{S - S_r}{S_s - S_r}, \tag{5}$$

where S_r is the residual saturation, S_s the fraction of water filled at full saturation (approximately equal to 1) and S is the degree of saturation.

Substituting the expression of effective degree of saturation (S_e) in eq. (4) yields the expression for effective stress of a partially saturated soil. Therefore, M-C shear strength for the unsaturated soil gets modified as

$$\tau_f = c' + [S_e(u_a - u_w) \tan \phi'] + (\sigma - u_a) \tan \phi'. \tag{6}$$

van Genuchten¹⁸ proposed a closed-form method for S_e based on the fitting parameters obtained from WRCC of a geomaterial.

$$S_e = \left\{ \frac{1}{1 + [\alpha(u_a - u_w)]^n} \right\}^m, \tag{7}$$

where α is the WRCC fitting parameter closely related to the inverse of AEV, n the WRCC fitting parameter related to the breadth of the pore-size distribution of the geomaterial and m is the symmetry parameter, related to n as $(1 - (1/n))$. Substituting the expression of S_e into eq. (6) yields the extended M-C failure criterion for an unsaturated geomaterial for a large range of matric suction incorporating the nonlinearity of strength.

Problem statement and material parameters

In the present study, probabilistic bearing capacity, considering the spatial variation of WRCC fitting curve parameters and angle of internal friction, has been evaluated. Figure 2 illustrates the schematic of the problem considered in the present study. Numerical analyses have been performed under a FELA framework, using the commer-

cially available software package OptumG2. For all numerical analyses, a rigid and rough strip footing of width $B = 1.0$ m has been considered. OptumG2 allows for an easy and intuitive modelling of the rigid behaviour of a geometry. An in-built option of 'Rigid' has been adopted from the material database of OptumG2, to simulate the rigid behaviour of the footing. A reduction factor of 1.0 was adopted to simulate a perfectly rough footing.

A kinematically admissible failure mechanism has been considered to yield the upper bound value of the true collapse load in all the analyses. As depicted through Figure 2, fly ash deposit of varying thickness has been assumed to be overlying natural soil deposit for the analyses. For *in situ* conditions, the fly ash deposit may be overlying a sand or a clay soil deposit and therefore, for a comprehensive study and to accommodate a large range of grain-size of soils, two different underlying soils, i.e. sand and clay have been considered for the study. The unsaturated behaviour of underlying clayey soil and granular soil has also been given due consideration. The lateral and bottom boundaries were fixed by running a number of trials so that the plastic zones during analysis do not extend up to the boundaries. Both horizontal and vertical fixities were applied to the bottom boundary, whereas the lateral boundaries were restricted against movement in the horizontal direction. The geomaterial within the problem boundary was discretized using triangular elements with upper-bound formulations. For enhancing the accuracy of the solution, an in-built function of 'mesh adaptivity', based on shear dissipation, was adopted. For mesh adaptivity, 10,000 start elements were considered. Finally, based on mesh sensitivity study, 10,000 elements were found to be adequate to satisfactorily model the behaviour of the footing. For the sake of brevity, results of mesh sensitivity are not presented here. Figure 3 shows the final finite element mesh of the system considered in this study.

For deterministic analyses, Table 1 summarizes the various input parameters adopted for both fly ash and natural soils (i.e. sand and clay). For fly ash, values are adopted from Prakash *et al.*², whereas for clay and sand

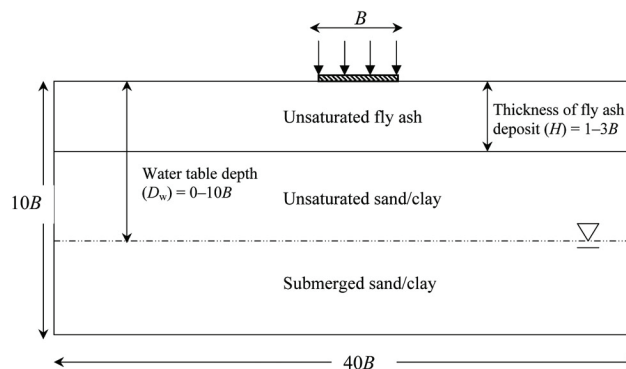


Figure 2. Schematic of the problem considered in the present study.

Table 1. Properties of geomaterials considered in this study for numerical modelling

Parameter	Values		
	Fly ash	Sand	Clay
Constitutive model	Mohr–Coulomb	Mohr–Coulomb	Tresca
Cohesion (c') (kPa)	0.1	0.1	–
Angle of internal friction (ϕ') ($^\circ$)	34	30	–
Undrained shear strength (S_u) (kPa)	–	–	44
vG parameter (α) (kPa $^{-1}$)	0.032	0.1	0.005
vG parameter (n)	2.161	4.0	1.8

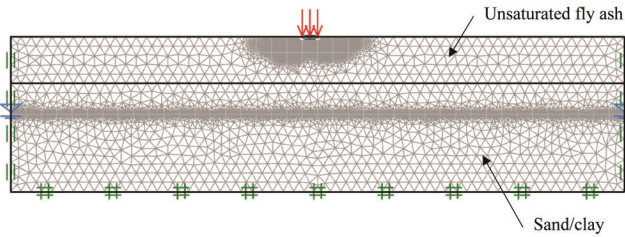


Figure 3. Finite element mesh of the system with boundary conditions considered in this study.

properties have been adopted from Vahedifard and Robinson¹², and Wu *et al.*²⁵ respectively. The M–C failure criterion was assumed to model the elastoplastic behaviour of sand and fly ash, whereas Tresca’s failure criterion was assumed to model the behaviour of clay.

Upper-bound finite element limit analysis

FELA was considered to obtain the upper-bound value of the collapse load. It is a powerful tool that conglomerates the inherent advantage of finite element discretization and brackets the true collapse load within an upper-bound and a lower-bound solution. For the present study, an upper-bound solution based on kinematically admissible failure mechanism was assumed. As already mentioned earlier, OptumG2 was used to carry out the analyses.

The basic idea behind an upper-bound analysis is that under an assumption of compatible mechanism of plastic deformation and kinematically admissible failure mechanism, the rate at which the external forces work would always be equal to or greater than the internal rate of dissipated energy²⁶. The virtual work expression governing the upper-bound failure mechanism may be expressed as^{26,27}

$$\int_{A_t} T_i \dot{u}_i dA + \int_V F_i \dot{u}_i dV \geq \int_V \sigma_{ij} \dot{\epsilon}_{ij} dV, \quad (8)$$

where T_i and F_i are surface and body loadings respectively, \dot{u}_i the velocity field kinematically compatible with the strain rate field $\dot{\epsilon}_{ij}$, σ_{ij} the actual stress field, and A_t and V are the surface area and volume of the domain respecti-

vely. In FELA, an adaptive mesh refinement technique is adopted, which equalizes $\int \gamma_{\max} dA$ (integral of the maximum shear strain rate, γ_{\max}) over the entire soil domain. After several iterations of adaptive refinement, the intensity of maximum shear strain (γ_{\max}) is revealed²⁸. In the present study, adaptive mesh refinement based on shear dissipation has been adopted to reveal the arrangement of plastic regions and velocity discontinuities.

Random field theory

The influence of inherent spatial variability associated with WRCC fitting parameters and angle of internal friction of fly ash is represented in terms of random field variations described by the mean, coefficient of variation (COV) and spatial correlation lengths considering log-normal distribution. Log-normal distribution has an inherent advantage that it guarantees a positive output and therefore is generally adopted to model the engineering properties of soils and rocks. Spatial variation of three different critical input parameters (WRCC parameters α , n and angle of internal friction ϕ') was modelled as log-normally distributed random fields². The standard deviation ($\sigma_{\ln \xi}$) and mean ($\mu_{\ln \xi}$) of any soil parameter ξ , may be derived as

$$\sigma_{\ln \xi} = \sqrt{\ln(1 + \text{COV}_\xi^2)}, \quad (9)$$

$$\mu_{\ln \xi} = \ln \mu_\xi - \frac{1}{2} \sigma_{\ln \xi}^2. \quad (10)$$

Similarly, the mean (μ_ξ), standard deviation (σ_ξ), median and mode of a log-normal distribution may be expressed as

$$\mu_\xi = e^{\left(\mu_{\ln \xi} + \frac{1}{2} \sigma_{\ln \xi}^2\right)}, \quad (11)$$

$$\sigma_\xi = \mu_\xi \sqrt{e^{\sigma_{\ln \xi}^2} - 1}, \quad (12)$$

$$\text{Median} = e^{\ln \xi}, \quad (13)$$

$$\text{Mode} = e^{(\mu_{\ln \xi} - \sigma_{\ln \xi}^2)}. \quad (14)$$

Probability distribution function (f) of a random soil parameter (ξ) may therefore be expressed as

$$f(\xi; \mu_\xi, \sigma_\xi) = \frac{1}{\xi \sigma_\xi \sqrt{2\pi}} e^{\left[\frac{-(\ln \xi - \mu_\xi)^2}{2\sigma_\xi^2} \right]} \quad (15)$$

To account for the spatial variation of soil parameters, anisotropic correlational lengths were used. Correlational lengths are presented in dimensionless forms by normalizing them with respect to the footing width (B) in both horizontal (L_x/B) and vertical (L_y/B) directions, where L_x and L_y are correlation length in the lateral and vertical directions respectively. To generate the random field and incorporate spatial variation of each random input parameter into the finite element limit analysis, Karhunen–Loeve (KL) expansion method was used. A total of 1000 terms in the KL expansion was used. A series of MCS was carried out for the assumed statistical properties of the input parameters. A sensitivity study was carried out to arrive at the number of MCS necessary to obtain the probabilistic mean value of bearing capacity with sufficient confidence and the Figure 4 shows results. On the basis of the results obtained through sensitivity analysis, it may be inferred that the mean value of bearing capacity ratio (BCR) (refer eq. (16)) converges to the deterministic BCR, for a MCS run exceeding 800. Also, it could be observed that even for 200 or more MCS runs, the difference in the results were well within $\pm 3\%$ and may be adopted for further analysis.

Figure 5 presents the framework of the present study.

Deterministic analysis

Deterministic analyses were carried out by assuming mean values of WRCC fitting parameters and angle of internal friction of the fly ash deposit (Table 1). Influence

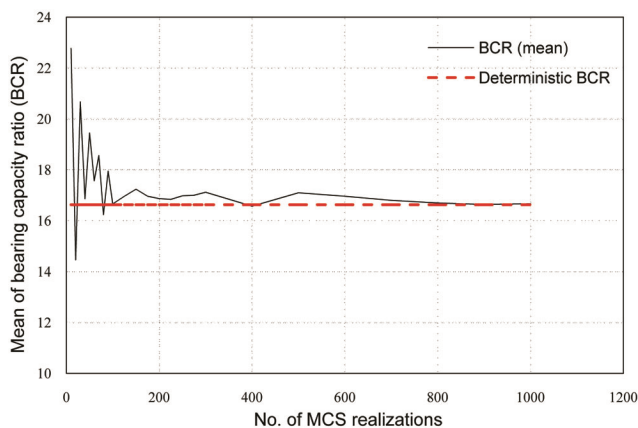


Figure 4. Sensitivity study on the number of Monte-Carlo simulations (MCS) for convergence.

of fluctuation of groundwater table depth (D_w) and thickness of fly ash deposit (H) on the bearing capacity was first evaluated. The threshold thickness of the fly ash deposit, beyond which the influence of the underlying soil diminishes, was obtained and used for subsequent analyses considering spatial variability of the fly ash deposit. The varying condition of matric suction due to fluctuation in the water table has been exclusively studied and reported for two different sub-soils (viz. sand and clay) separately based on their different inherent WRCC parameters. An upper-bound limit of true collapse load was obtained and the results have been presented in terms of a dimensionless form as BCR defined as

$$BCR = \frac{P_u}{\gamma B}, \quad (16)$$

where p_u is the upper-bound of true collapse load, γ the saturated unit weight of fly ash and B is the width of the footing.

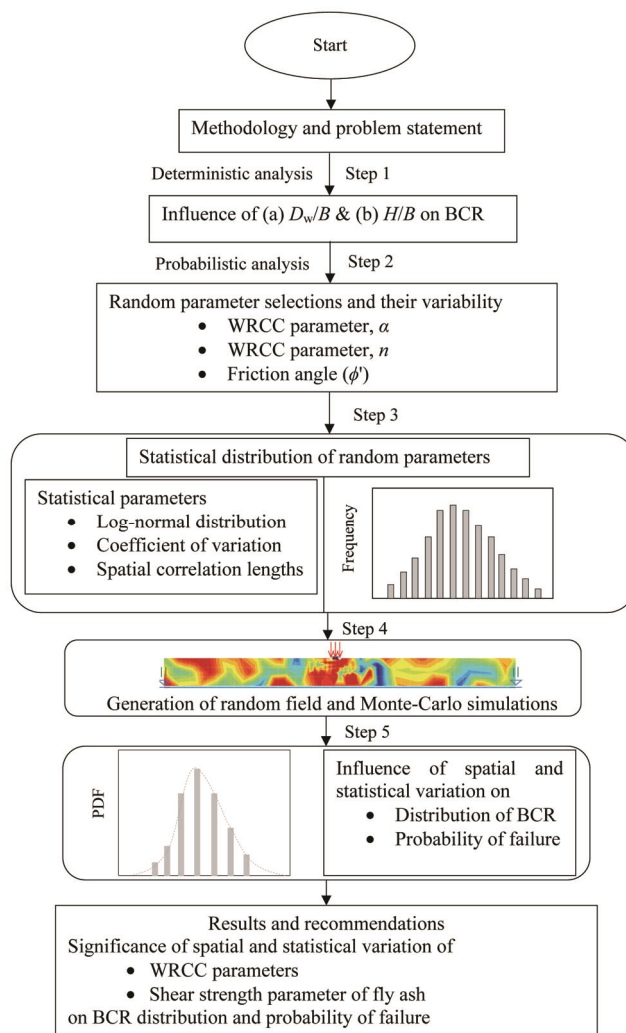


Figure 5. Framework of the present study.

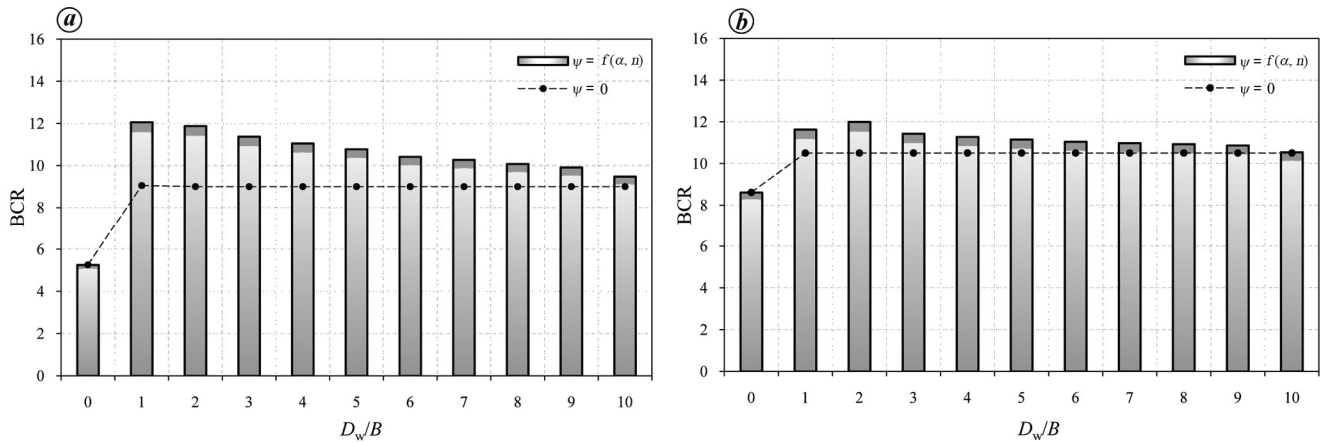


Figure 6. Variation of BCR with D_w/B for fly ash deposit with and without matric suction (ψ) when it is overlying (a) sand and (b) clay.

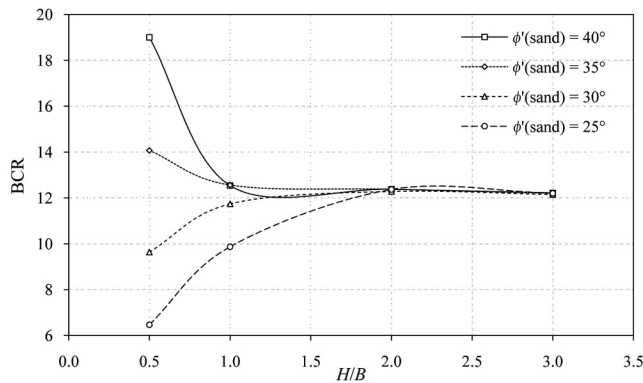


Figure 7. Variation of BCR with H/B for fly ash deposit considering the underlying sand.

Influence of water table depth on BCR

In this section we discuss the influence of fluctuation of groundwater table depth ratio (D_w/B) on BCR of the footing. For comparative purposes, influence of groundwater table (GWT) fluctuation was incorporated with and without the matric suction (ψ) of the geomaterial above GWT. For the analysis, a thickness ratio (H/B) of 0.5 was assumed for the fly ash deposit. Figure 6 depicts the variation of BCR with D_w/B .

It may be observed from the figure that by neglecting the matric suction above GWT, BCR of the footing is underestimated. This observation holds good for both sand and clay as underlying materials. When $D_w/B = 0$, matric suction is absent, and therefore BCR is same for both the cases, with and without suction. However, when unsaturation is considered, BCR increases with D_w/B and reaches a maximum value for D_w/B of approximately 1–2. With a further drop in GWT, BCR reduces gradually and attains a constant value. The BCR behaviour of fly ash overlying both clay and sand is observed to be almost identical.

This could be attributed to the fact that when GWT level decrease, the degree of saturation of the soil within the influence zone of the footing also decreases. This results in an increase in matric suction (refer to Figure 1) and subsequently an increase in BCR. However, when GWT further decreases, the degree of saturation tends to become equal to the residual saturation (i.e. $S = S_r$). Consequently, the contribution of matric suction on the overall bearing capacity ceases to exist (refer to eqs (5) and (6)).

Influence of thickness of fly ash deposit

Fly ash overlying coarse-grained soil (sand): To comprehensively study the influence of thickness ratio (H/B) of the unsaturated fly ash deposit on BCR, deterministic analyses have been carried out. For all the analyses, D_w/B was assumed to be 10 to minimize the influence of GWT. For the analyses, four different magnitudes of friction angle of sand ($\phi'_{\text{sand}} = 25^\circ, 30^\circ, 35^\circ$ and 40°) have been considered. Figure 7 presents the variation of BCR with thickness of the fly ash deposit overlying sand. As evident from the figure, the influence of the underlying sand layer diminishes as the thickness ratio (H/B) exceeds a value of more than 2.0 within the range of friction angles considered for sand. When H/B is less than 2.0, BCR is substantially affected by the friction angle of the underlying soil. From Figure 7, it may be observed that for higher friction angle of sand, BCR decreases as the thickness of the fly ash deposit increases. On the other hand, for sand layer with smaller friction angles, BCR tends to increase with increase in the thickness of the fly ash deposit. This can be explained by the fact that for lesser thickness of the fly ash deposit ($H/B < 2.0$), the failure mechanism penetrates deeper within the sand layer. Consequently, BCR is affected by the friction angle of the underlying soil. The influence of the underlying sand layer diminishes for fly ash thickness of more than $2.0B$.

Table 2. Mean, standard deviation and coefficient of variance of input parameters

Parameter	Values			
	Mean	Standard deviation	Coefficient of variance (%)	Distribution
vG (1980) parameter (α) (kPa ⁻¹)	0.032	0.015	47	Log-normal
vG (1980) parameter (n)	2.161	0.574	26.5	Log-normal
Angle of internal friction (ϕ') (°)	34	3.63	10.67	Log-normal

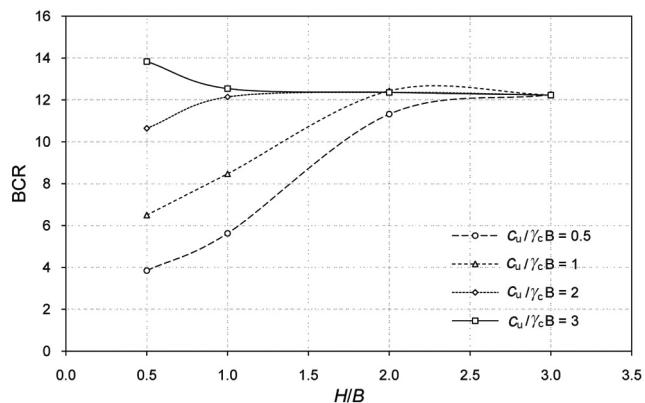


Figure 8. Variation of BCR with H/B for fly ash deposit considering the underlying clay.

Fly ash overlying fine-grained soil (clay): It may often be possible that a fly ash fill is constructed over fine-grained soil such as clay. In such a case, the bearing behaviour of the footing will be inherently different. This difference in the bearing behaviour predominantly arises due to inherently different water retention characteristics of sand and clay. In the present study, five different undrained shear strength ratios ($c_u/\gamma_c B = 0.5, 1.0, 2.0$ and 3.0 , where c_u is the undrained cohesion and γ_c is the unit weight of clay) have been considered. Figure 8 presents the variation of BCR with H/B and ($c_u/\gamma_c B$). As depicted in figure, BCR tends to attain a constant value for H/B more than 2.0. Similar observations were also made for coarse-grained soil (Figure 7). Therefore, for a water table depth ratio of $10B$, the influence of the underlying soil on BCR diminishes for H/B value of 2.0 or more. Hence, for all the probabilistic analyses, $H/B = 3.0$ has been assumed to eliminate the influence of the underlying soil on BCR. It may be observed that BCR is lower for smaller values of undrained shear strength of clay with lesser thickness of fly ash deposit. For a constant fly ash thickness ratio, BCR tends to increase with increase in the undrained shear strength of clay.

Probabilistic analyses

In this section, we discuss the effects of spatial variation of random parameters on BCR of unsaturated fly ash deposit. As discussed before, based on a sensitivity study, 200 M-C simulations were carried out to obtain the prob-

abilistic distribution of BCR. The KL expansion method was used to generate the random field for all the random input parameters based on the mean and variance values as summarized in Table 2 and adopted from Anand and Sarkar²⁹, and Prakash *et al.*². As already mentioned the influence of the underlying layer is minimal for a thickness ratio of more than 2.0; therefore $H/B = 3.0$ was adopted for all the probabilistic analyses to minimize the influence of the underlying deposit. GWT depth was fixed at a constant value of $3.0B$ for all the analyses. In the present study, deterministic stiffness parameters of the fly ash deposit have been considered. For random field analyses, different combinations of correlational lengths ($L_x = 1-5B$ and $L_y = 1-5B$) were assumed for each random parameter for both vertical and horizontal directions.

Influence of spatial variation of WRCC parameter (α)

As already discussed, the shear strength of a geomaterial under an unsaturated framework substantially depends on the magnitude of AEV (or α) of the geomaterial (eqs (6) and (7)). Vahedifard and Robinson¹² proposed a closed-form expression for ultimate bearing capacity (q_u) of a shallow strip footing resting over a variably saturated soil media as

$$q_u = \left\{ c' + \frac{1}{\alpha} (1 - S_{e,AVR}) \tan \phi' + \sigma_{AVR}^s \right\} N_c + q N_q + \frac{1}{2} \gamma_{av} B N_\gamma, \tag{17}$$

where $S_{e,AVR}$ is the average effective degree of saturation within the pressure bulb of the footing, σ_{AVR}^s the contribution of the average suction stress beyond the air-entry pressure, γ_{av} the modified average unit weight, q the overburden pressure, and N_c, N_q and N_γ are Terzaghi's³⁰ bearing capacity factors.

However, an accurate and reliable determination of α is difficult and bearing capacity analysis based on a single value of α may not yield a reliable bearing capacity value. Moreover, the value of α may vary spatially due to improper compaction control, and several depositional and post-depositional processes. Therefore, we discuss the influence of spatial variation of α on the statistical distribution of bearing capacity of the shallow strip footing. The van Genuchten¹⁸ parametric model was used for modelling the unsaturated behaviour of fly ash. While considering

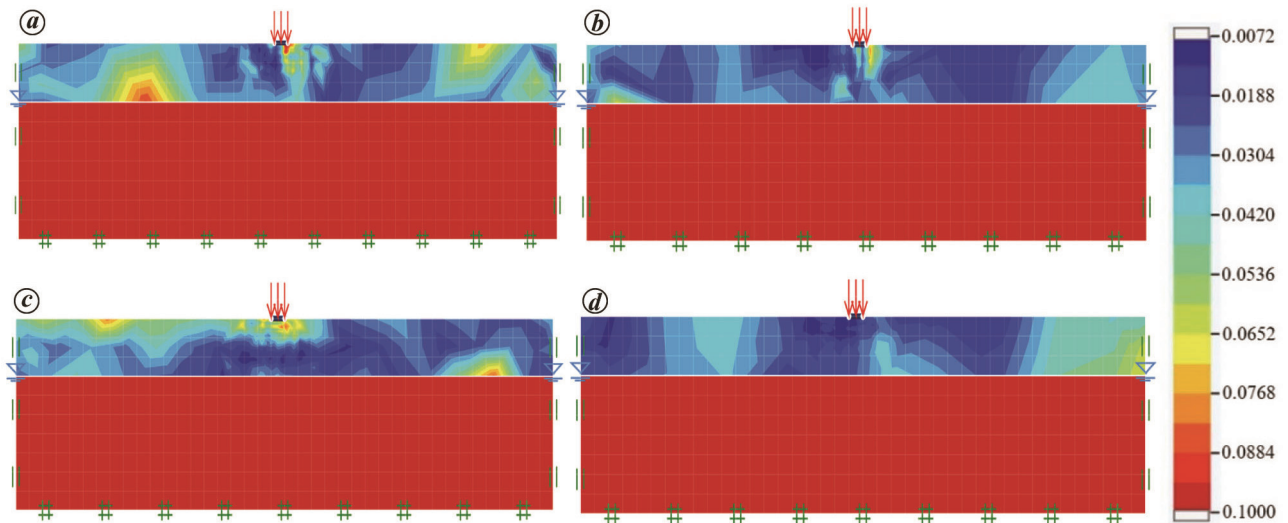


Figure 9. Typical spatial variation of α for (a) $L_x = 1B$ and $L_y = 1B$, (b) $L_x = 1B$ and $L_y = 5B$, (c) $L_x = 5B$ and $L_y = 1B$ and (d) $L_x = 5B$ and $L_y = 5B$.

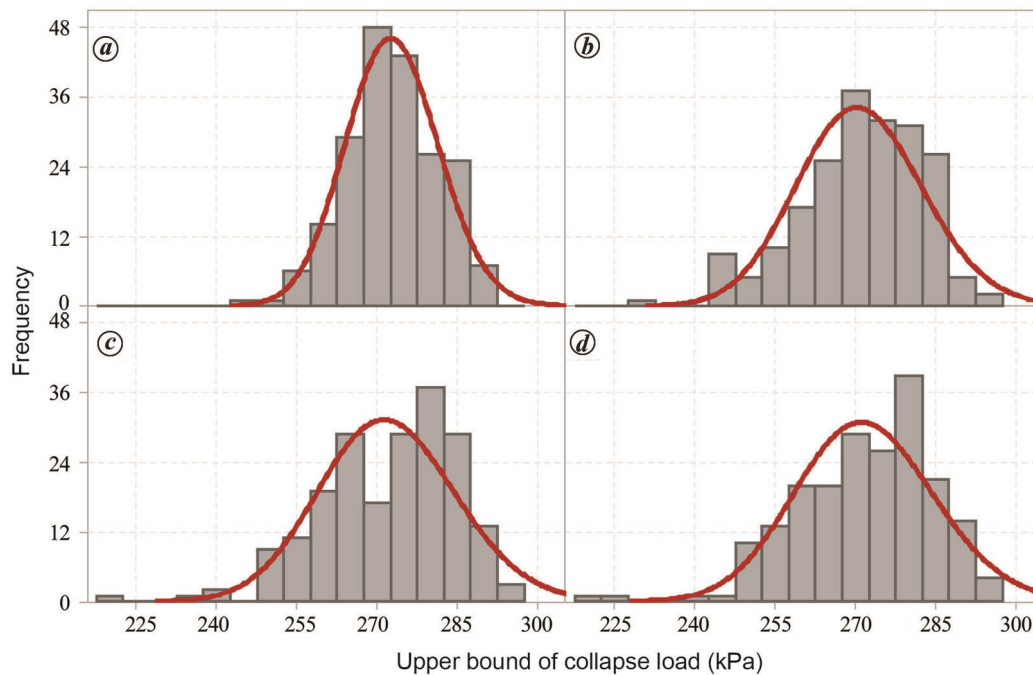


Figure 10. Variation of bearing capacity with various spatial correlational lengths of parameter α : (a) $L_x = 1B$ and $L_y = 1B$, (b) $L_x = 2B$ and $L_y = 2B$, (c) $L_x = 3B$ and $L_y = 3B$ and (d) $L_x = 4B$ and $L_y = 4B$.

the random statistical variation of α , values of all other critical input parameters were kept constant to their mean values. As mentioned earlier, to incorporate spatial variation, different combinations of correlational lengths were assumed. Figure 9 demonstrates the typical random fields generated for α .

The distribution of bearing capacity has been presented in terms of a histogram output and a lognormal fitting of the bearing capacity of fly ash deposit was obtained. For brevity, in Figure 10, probability distribution function (PDF) of bearing capacity is shown for only four isotropic

correlational lengths of α . As can be observed from the figure, with increase in the isotropic correlational lengths, PDF of the bearing capacity is slightly skewed towards the right. It may be mentioned that with increase in the isotropic correlational lengths, mean value of the bearing capacity shows a slight increase. However, as evident from Figure 10, standard deviation shows a substantial increase with increase in isotropic correlation length. This can be explained by the fact that for small correlational lengths, parameters are weakly correlated over the potential failure surface. However, fluctuations of the parameters have been

averaged to a mean value along the potential failure surface (also known as ‘averaging effect’; for more details readers may refer to Cho and Park³¹). Therefore, for small correlational lengths, ‘averaging effect’ was more and consequently mean and deviation of the bearing capacity distribution of fly ash deposit were less. As the correlational length increases, the ‘averaging effect’ is reduced and hence the mean and deviation tend to increase.

The probability of failure (P_f) of the footing was evaluated as given below.

$$P_f = \frac{\sum_{i=1}^N \Theta \left(\frac{BCR_d}{BCR_i} \right)}{N}, \quad (18)$$

where BCR_d is the deterministic bearing capacity ratio assuming mean values of each parameter, BCR_i the bearing capacity ratio obtained from the i th MCS, N is the total number of MCS runs, Θ is a function which returns a value of ‘1’ if the argument is more than unity, else it returns ‘0’. Figure 11 presents the variation of P_f with isotropic spatial correlational length. For a comprehensive analysis, a wide range of isotropic spatial correlational lengths ($L_{xy}/B = 0.25, 0.5, 1, 2, 3, 4, 5, 10, 20, 30, 40$ and 50) have been considered (where L_{xy} denotes isotropic spatial correlation length, i.e. $L_x = L_y$).

It may be observed from the figure that for lesser isotropic spatial correlation length, P_f is smaller. This could be attributed to the fact that for lesser spatial correlation lengths, the preferential weak path of failure becomes more circuitous. Therefore, due to the ‘averaging effect’, the mean failure path would be identical as in the case of a homogeneous fly ash with mean value of its parameters³². Therefore, for smaller isotropic correlation lengths, mean of the bearing capacity tends to attain a deterministic value and therefore P_f tends to become 50%. The proba-

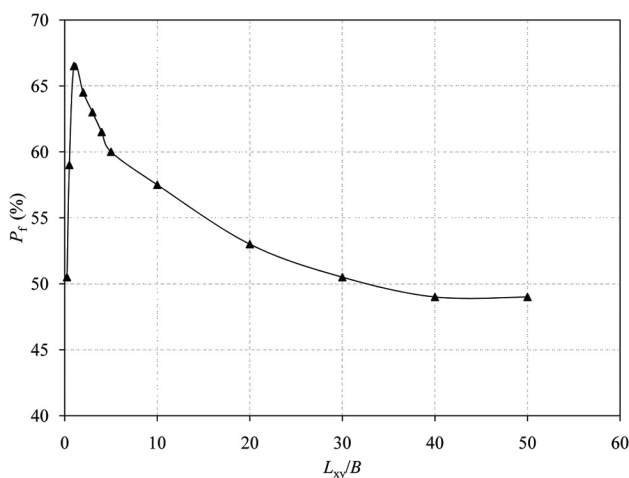


Figure 11. Variation of probability of failure (P_f) with spatial isotropic correlation length (L_{xy}/B) of α .

bility of failure was found to be greater when the spatial correlation length was between 0.5 and 5, and may be referred to as the ‘worst case correlation length’. The change in probability of failure in this range of correlation is quite significant. With further increase in correlation length, P_f reduces gradually as the heterogeneity of fly ash diminishes and tends to attain a P_f value of 50% for larger values of L_{xy} . To incorporate the influence of anisotropy of correlation length in this study, 5×5 different anisotropic cases have been considered. For these analyses, spatial correlation lengths lying within the ‘worst case correlation lengths’ are only considered. Figure 12 presents the variation of P_f with spatial correlation lengths in contour form for α . As is evident from the figure, with an increase in correlation length (for both isotropic and anisotropic), P_f reduces and tends to attain a minimum value for higher correlation lengths.

Influence of spatial variation of WRCC parameter (n)

Parameter n represents the slope at the inflection point of the WRCC curve. It is closely related to the rate of desorption or drying. n also represents the breadth of pore size distribution of a geomaterial³³ and is inversely related with the pore-size distribution. Conventionally, its value lies between 1.1 and 8.5 for all natural soils¹⁸. For sand or coarse-grained soil, n would be high compared to that of a fine-grained soil²³. An accurate measurement of n requires collection of a large number of experimental data. Moreover, accurate determination of n demands proper fitting of the parametric model (such as the van Genuchten¹⁸ model) to a limited number of test data. In view of these limitations, here we discuss the influence of uncertainty in n on the bearing behaviour of the shallow footing. A random field was generated under finite element framework and n was considered as a spatially varying

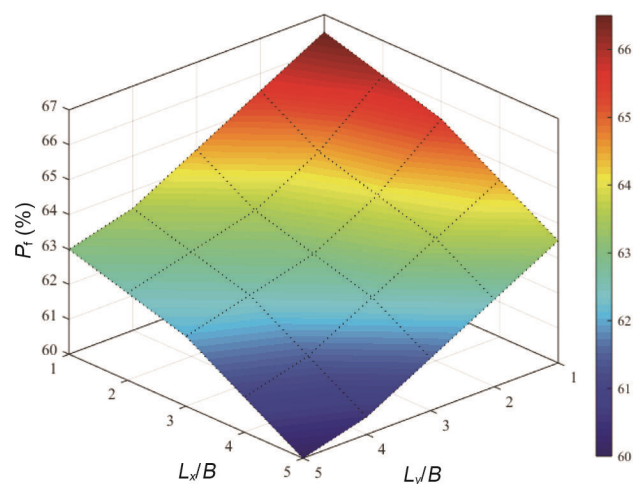


Figure 12. Contour variation of P_f with anisotropic spatial correlation lengths of α .

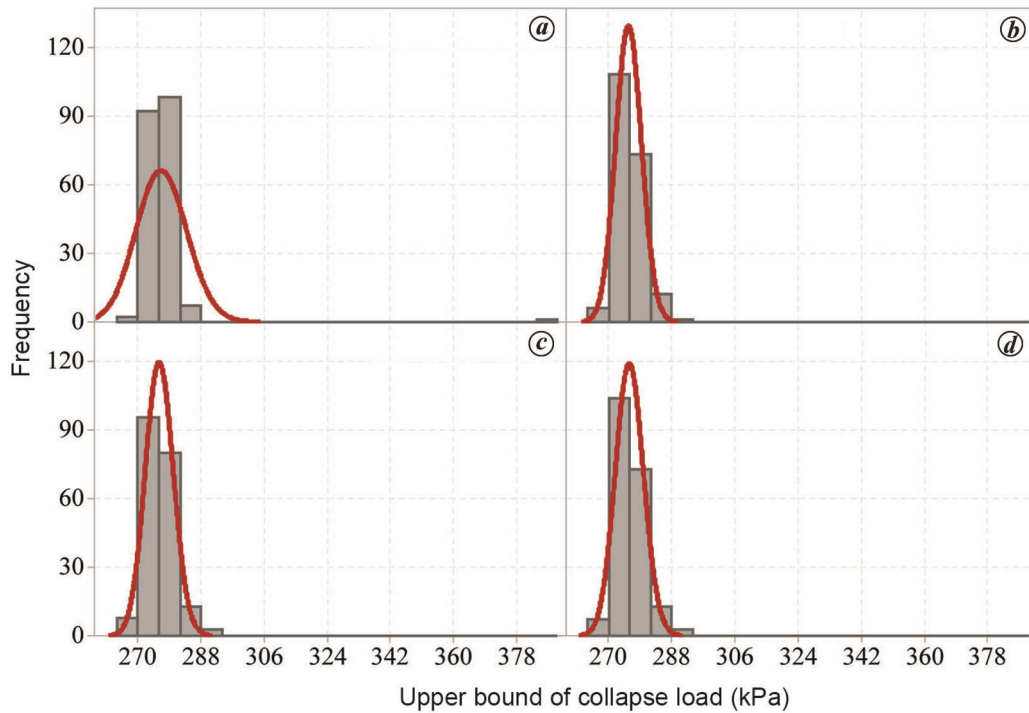


Figure 13. Variation of bearing capacity with various spatial correlational lengths of parameter n : (a) $L_x = 1B$ and $L_y = 1B$, (b) $L_x = 2B$ and $L_y = 2B$, (c) $L_x = 3B$ and $L_y = 3B$ and (d) $L_x = 4B$ and $L_y = 4B$.

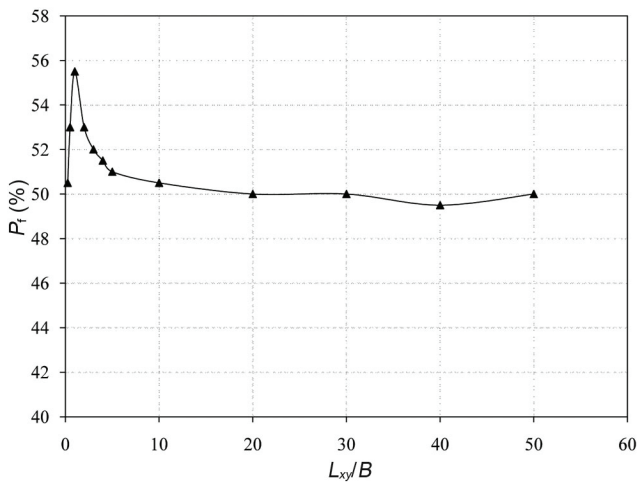


Figure 14. Variation of probability of failure (P_f) for spatial isotropic correlation lengths (L_{xy}/B) of parameter n .

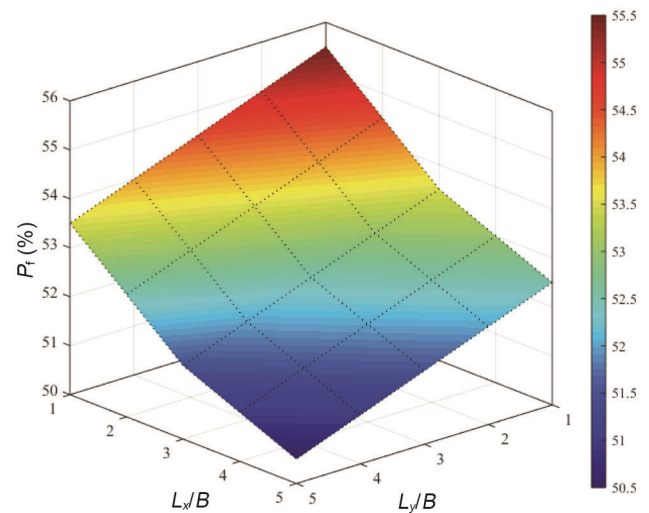


Figure 15. Contour variation of P_f with anisotropic spatial correlation lengths of parameter n .

random field parameter with mean and COV_n (Table 2). Figure 13 presents the PDF of bearing capacity of the fly ash deposit due to spatial variation of n .

Like the case of α , variation of P_f was obtained for a wide range of isotropic correlation lengths for n . Figure 14 presents the variation of probability of failure with correlation length. It may be observed from the figure that the influence of n on the probability of failure is comparatively insignificant for COV_n and correlation

lengths considered in this study. Therefore, based on the present observations, it may be hypothesized that the influence of uncertainty in the random input parameter n does not have any significant impact on the probability of failure. The initial increase in the probability of failure is majorly due to the ‘averaging effect’, as already discussed earlier.

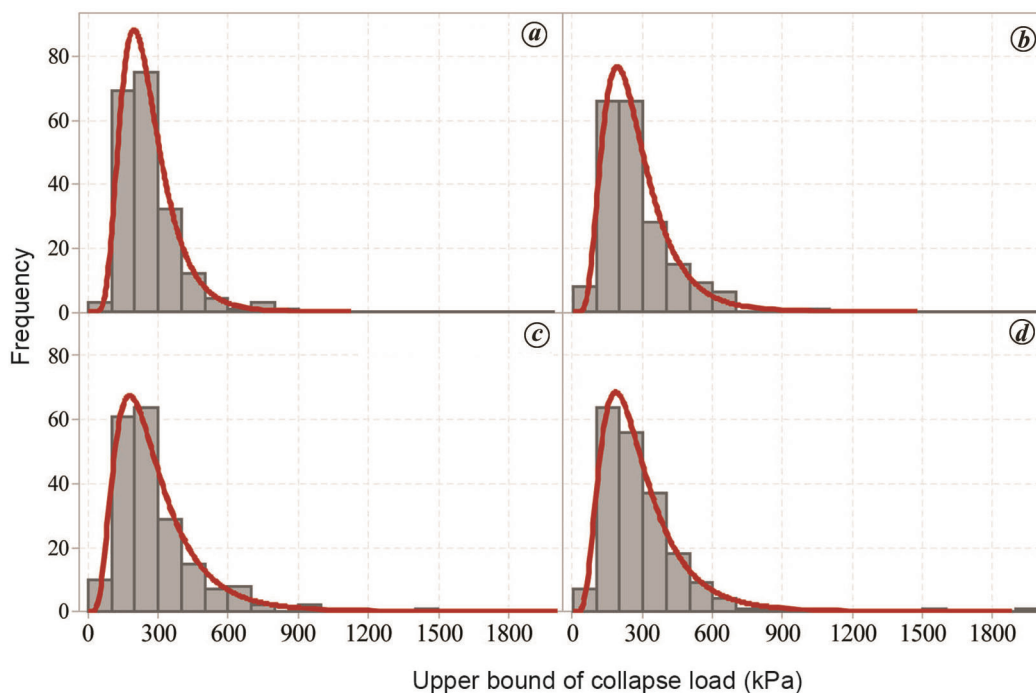


Figure 16. Variation of bearing capacity with various spatial correlational lengths of friction angle ϕ' : (a) $L_x = 1B$ and $L_y = 1B$, (b) $L_x = 2B$ and $L_y = 2B$, (c) $L_x = 3B$ and $L_y = 3B$, and (d) $L_x = 4B$ and $L_y = 4B$.

Figure 15 presents the contour variation of P_f with spatial correlation length of n . It may be observed from the figure that the probability of failure is relatively high for small values of spatial correlation lengths, and attains a minimum value for higher correlation lengths. This implies that the increase in homogeneity of fly ash indicates an increase in correlation length, and the mean value of the bearing capacity tends to attain a specific constant value.

Influence of spatial variation of angle of internal friction (ϕ')

As the angle of internal friction (ϕ') is the most critical parameter for a cohesionless fly ash deposit, therefore, in this section, the influence of anisotropic spatial variation of angle of internal friction on the response of bearing capacity of fly ash deposit is discussed. Figure 16 presents the distribution function of bearing capacity for four different isotropic spatial correlation lengths.

The figure presents PDFs obtained by considering four isotropic spatial correlational lengths ($L_{xy}/B = 1, 2, 3$ and 4). It can be observed that the variance of the bearing capacity is less for smaller isotropic correlational lengths. On the contrary, for large correlational lengths, the variance is higher. Moreover, the mean value of bearing capacity increases with increase in isotropic correlation lengths. This may be mainly attributed to the fact that for small correlational lengths, the soil is more heterogeneous and the random field generated is more non-uniform. However, as the spatial correlational length increases, spatial varia-

tion of ϕ' becomes less and tends to become uniform with gradual increase in correlational length. Similar to the other parameters, probability of failure for spatial variation of angle of internal friction was evaluated for various isotropic correlation lengths (Figure 17). It can be observed from Figure 17 that due to heterogeneity arising from the spatial variation of angle of internal friction, the probability of failure fluctuates substantially. It gradually reduces with reduction in spatial heterogeneity and tends to attain a minimum value for large spatial correlational lengths. Figure 18 shows the contour variation of P_f with spatial correlation length of friction angle.

Next we present the variation of bearing capacity of the fly ash deposit considering the spatial variability of the WRCC parameters and friction angle of the deposit. The bearing capacity was significantly influenced by the spatial variation of these parameters. For each random parameter, probability of failure (P_f) was significantly higher for smaller correlational lengths. Therefore, if the values of the parameters exhibit high variability within small ranges of distance, then the probability of a lesser value of the bearing capacity of the footing is substantially higher. Therefore, if a structural fill exhibits significant variability within a short length, then a conservative design of the footing may be adopted.

Parametric study

In the previous sections, the bearing capacity of the fly ash deposit was studied for a constant value of mean and

COV of the parameters. Although the mean and COV of the parameters adopted in the present study are representative of the values obtained during *in situ* conditions², a more comprehensive study necessitates accounting for the influence of variation in COV of all the three critical input parameters (viz. COV_{α} , COV_n and COV_{ϕ}) on the overall distribution of the bearing capacity (or probability of failure). A parametric variation of COV of all the three critical random input parameters was considered in the present study and their consequent impacts on the probability distribution was obtained. For brevity, results are presented only in terms of variation of P_f with COV. Five different COV values ($COV = 10\%$, 20% , 30% , 40% and 50%) have been considered for each parameter^{34–36}. All other input parameters, geo-hydrological configuration

(i.e. depth of water table) and boundary values (thickness ratio) were kept constant.

WRCC parameter (α): Variation of probability of failure (P_f) with different COV_{α} values and isotropic correlational lengths was evaluated. Figure 19 presents the results. Variation of probability of failure with α may be explained with the help of eqs (6) and (7). Under an unsaturated framework, the shear strength depends significantly on WRCC α . Therefore, statistical variation in α would most certainly affect the distribution of the bearing capacity and therefore, the probability of failure of the footing would change. As shown in Figure 19, with an increase in COV_{α} , probability of failure increases steeply for lower COV values. Then, it increases gradually for higher COV values. This may be explained by the fact that increase in COV_{α} imparts higher heterogeneity to the field. For small values of COV_{α} , the mean bearing capacity tends to approach the value considering a homogeneous layer and consequently, the probability of failure is low. However, as the heterogeneity increases due to increase in COV_{α} , the variance in the distribution of the bearing capacity is greater and the mean value of the bearing capacity becomes less. This leads to consequent increase in the probability of failure of the footing. For very high values of COV_{α} , this effect is neutralized and consequently, the increase in probability of failure is rather gradual. Moreover, it may be noticed that the variation of probability of failure diminishes with increase in the isotropic spatial correlational lengths (Figure 19). This may be chiefly attributed to the enhanced homogeneity in fly ash with increase in correlational lengths.

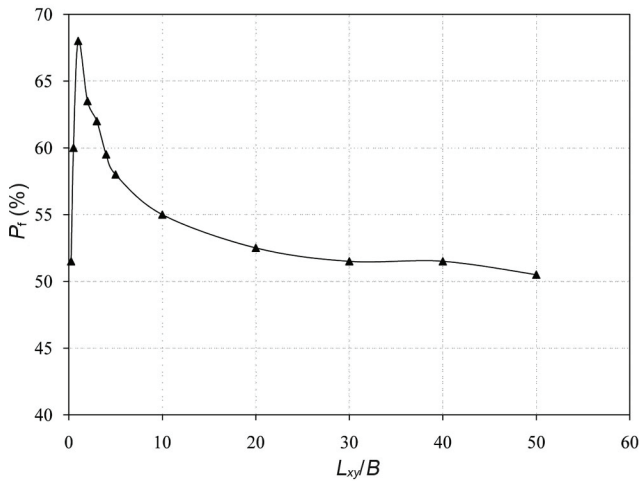


Figure 17. Variation of probability of failure (P_f) for spatial isotropic correlation lengths (L_{xy}/B) of friction angle ϕ' .

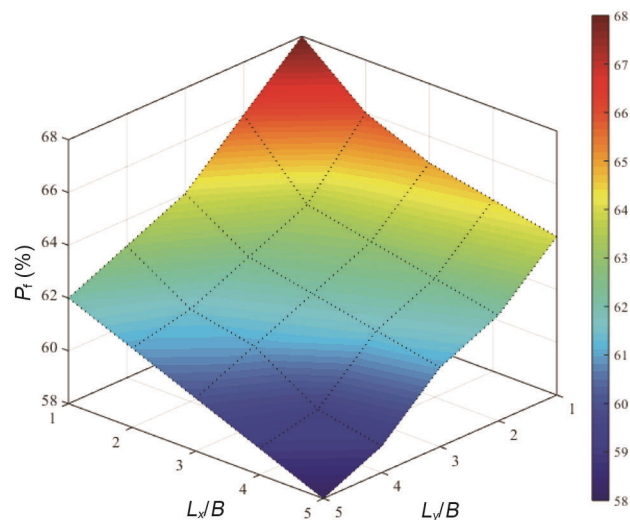


Figure 18. Contour variation of P_f with anisotropic spatial correlation lengths of friction angle ϕ' .

WRCC parameter (n): Figure 20 shows the influence in the variability of n on P_f . As already shown in eqs (6) and (7), under the unsaturated framework, shear strength of a

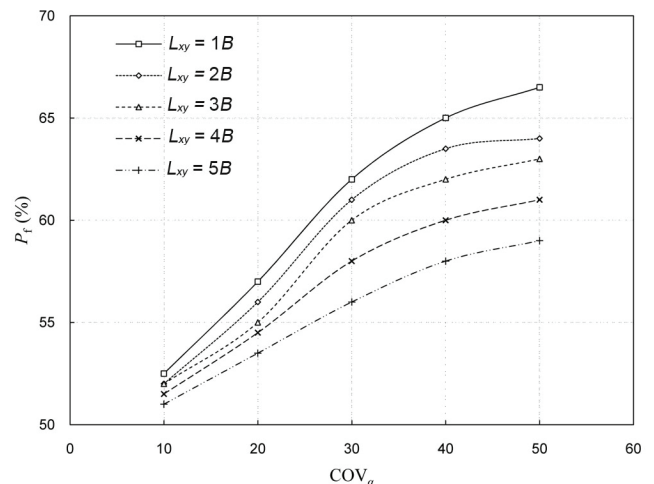


Figure 19. Variation of P_f with COV_{α} for isotropic spatial correlation lengths.

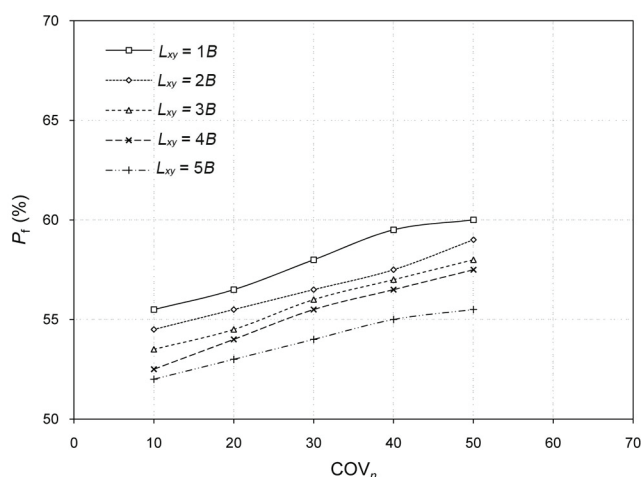


Figure 20. Variation of P_f with COV_n and isotropic spatial correlational lengths.

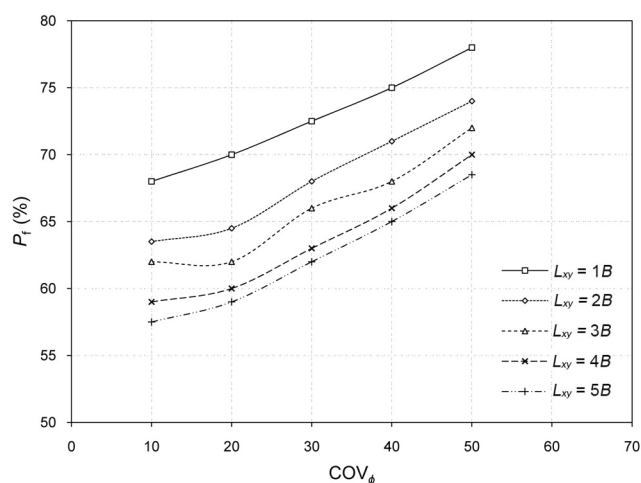


Figure 21. Variation of P_f with COV_ϕ and isotropic spatial correlational lengths.

geomaterial is a function of n . Parameter n represents the rate of desorption of the geomaterial upon desaturation in WRCC. The value of n is generally high for coarse-grained soils and low for fine-grained soils. It may be observed from Figure 20 that with the increase in COV_n , P_f increases due to the widening of the statistical distribution of the bearing capacity. A quick quantitative comparison between Figures 19 and 20 suggests that the variation of P_f due to n is less significant than the variation of α for identical ranges of COV values considered. This suggests that the variation of BCR is less sensitive to variation in n compared to α .

Angle of internal friction of fly ash (ϕ'): Figure 21 shows the variation of the probability of failure with COV_ϕ . As the shear strength and bearing capacity of the geomaterial are governed by ϕ' , substantial impact on BCR was anticipated due to variation in the distribution of ϕ' . It may

be observed from the figure that for all the COV_ϕ values considered in the present study, P_f increases gradually with increase in COV_ϕ for all the isotropic correlation lengths. Hence from these parametric analyses, it can be inferred that the spatial variation of WRCC parameters and the strength parameter of the fly ash deposit play a significant role on the bearing behaviour of the footing.

Summary and conclusion

Deterministic analyses were carried out to obtain the influence of fluctuation in the groundwater table (D_w/B) and thickness ratio (H/B) of a fly ash deposit on the bearing capacity. The analyses were carried out for two different underlying soils, i.e. sand and clay under an unsaturated framework. The threshold thickness and influence of matric suction on the bearing capacity were determined. A practising civil engineer may find these results helpful

while designing a shallow foundation over a fly-ash fill that is resting on a clay/sand deposit and subjected to varying groundwater table fluctuations.

A probabilistic analysis on the bearing capacity of a rigid, rough, strip footing on a partially saturated and spatially variable fly ash deposit has also been presented. The variability of fly ash parameters was incorporated in terms of COV and the spatial anisotropic correlational lengths (L_x and L_y). Random field theory was used with nonlinear EFLA to obtain the statistical distribution of the upper-bound value of bearing capacity, in conjunction with M–C simulations. The study may be summarized as below.

- Strength nonlinearity of geomaterials arising from partial saturation of the pore matrix and its variation due to fluctuation in GWT and WRCC parameters substantially influence the bearing capacity. The present study incorporates a two-layered problem with partial saturation behaviour fly ash.
- Results reported in this study would be beneficial while estimating the thickness of fly ash required for structural fill under varying fluctuations of GWT and for different underlying soils.
- The present study examines the bearing capacity of fly ash deposit considering the random field variation (or spatial variation) of WRCC fitting parameters and the shear strength parameter. The bearing behaviour was substantially sensitive to spatial variation of WRCC fitting parameters (α and n) within the range of spatial correlation lengths and the statistical values adopted. Sensitivity of angle of internal friction on the statistical bearing capacity was also found to be significant. For increase in spatial correlation lengths from $1B$ to $5B$, the percentage reduction in P_f was 9.78%, 8.11% and 14.7% for α , n and ϕ' respectively.
- For very small correlation lengths (smaller than $1B$), due to averaging effect, probability of failure (P_f) was small. However, it increased up to a correlational length ratio of $1B$. Probability of failure decreased with increase in spatial correlation lengths for values larger than $1B$.
- For each random input parameter, P_f increased with increase in the coefficient of variation of the parameters. For small correlational lengths, P_f decreased and attained a minima. Influence of COV on bearing capacity was most sensitive for angle of internal friction and least for WRCC parameter n . For example, for $L_{xy} = 1B$, the probability of failure varied within the range 68–78% for variation in COV_ϕ . For the same correlation length $L_{xy} = 1B$, P_f varied within the range 55–60% with COV_n . For α ($L_{xy} = 1B$), P_f variation was in the range 53–67%.
- For equal increase in the COV values of parameters α , n and ϕ' , maximum percentage increment in the probability of failure was 26.7%, 8.1% and 19.13% respec-

tively. Thus, the maximum rate of increase in P_f with COV was highest for α , followed by ϕ' and n .

- Finally, the effects of spatial variations of WRCC parameters and strength parameters on the bearing capacity of the fly ash deposit would help designers to plan and carry out adequate geotechnical engineering investigations at the project site.

1. Nadaf, M. B. and Mandal, J. N., Behaviour of reinforced fly ash slopes with cellular mattress and strips under strip loading. *J. Hazard. Toxic Radioact. Waste*, 2017, **21**(4); [https://doi.org/10.1061/\(ASCE\)HZ.2153-5515.0000376](https://doi.org/10.1061/(ASCE)HZ.2153-5515.0000376).
2. Prakash, A., Hazra, B. and Sreedeeep, S., Probabilistic analysis of unsaturated fly ash slope. *J. Hazard. Toxic Radioact. Waste*, 2019, **23**(1); [https://doi.org/10.1061/\(ASCE\)HZ.2153-5515.0000428](https://doi.org/10.1061/(ASCE)HZ.2153-5515.0000428).
3. Wang, D., Tawk, M., Indraratna, B., Heitor, A. and Rujikiatkamjorn, C., A mixture of coal wash and fly ash as a pavement substructure material. *Transp. Geotech.*, 2019, **21**, 100265; <https://doi.org/10.1016/j.trgeo.2019.100265>.
4. Bhatia, R. and Kumar, A., Load-settlement behavior of concrete debris pile in fly ash fill. *J. Hazard. Toxic Radioact. Waste*, 2020, **24**(3), 04020006; [https://doi.org/10.1061/\(ASCE\)HZ.2153-5515.0000494](https://doi.org/10.1061/(ASCE)HZ.2153-5515.0000494).
5. Pant, A., Ramana, G. V., Datta, M. and Gupta, S. K., Comprehensive assessment of cleaner, sustainable and cost-effective use of coal combustion residue (CCR) in geotechnical applications. *J. Clean. Prod.*, 2020, **271**, 122570; <https://doi.org/10.1016/j.jclepro.2020.122570>.
6. Bhatt, A., Priyadarshini, S., Mohankrishnan, A. A., Abri, A., Sattler, M. and Techapaphawit, S., Physical, chemical, and geotechnical properties of coal fly ash: a global review. *Case Stud. Constr. Mater.*, 2019, **11**; <https://doi.org/10.1016/j.cscm.2019.e00263>.
7. Fredlund, D. G. and Morgenstern, N. R., Stress state variables for unsaturated soils. *J. Geotech. Eng. Div. Am. Soc. Civ. Eng.*, 1977, **103**, 447–466; <https://doi.org/10.1061/AJGEB6.0000423>.
8. Fredlund, D. G., Morgenstern, N. R. and Widger, R. A., The shear strength of unsaturated soils. *Can. Geotech. J.*, 1978, **15**(3); <https://doi.org/10.1139/t78-029>.
9. Fredlund, D. G. and Rahardjo, H., *Soil Mechanics for Unsaturated Soils*, Wiley, New York, USA, 1993, p. 517; <https://doi.org/10.1002/9780470172759>.
10. Oloo, S. Y., Fredlund, D. G. and Gan, J. K. M., Bearing capacity of unpaved roads. *Can. Geotech. J.*, 1997, **34**(3), 398–407; <https://doi.org/10.1139/t96-084>.
11. Xu, Y., Bearing capacity of unsaturated expansive soils. *J. Geotech. Geol. Eng.*, 2004, **22**, 611–625; <https://doi.org/10.1023/B:GEGE.0000047043.29898.17>.
12. Vahedifard, F. and Robinson, J. D., Unified method for estimating the ultimate bearing capacity of shallow foundations in variably saturated soils under steady flow. *J. Geotech. Geoenviron. Eng.*, 2016, **142**(4), 04015095; [https://doi.org/10.1061/\(ASCE\)GT.1943-5606.0001445](https://doi.org/10.1061/(ASCE)GT.1943-5606.0001445).
13. Vanapalli, S. K. and Mohamed, F. M. O., Bearing capacity of model footings in unsaturated soils. In *Experimental Unsaturated Soil Mechanics* (ed. Schanz, T.), Springer, Berlin, Germany, 2007, pp. 483–493; https://doi.org/10.1007/3-540-69873-6_48.
14. Vanapalli, S. K., Fredlund, D. G., Pufahl, D. E. and Clifton, A. W., Model for the prediction of shear strength with respect to soil suction. *Can. Geotech. J.*, 1996, **33**(3), 379–392; <https://doi.org/10.1139/t96-060>.
15. Zhang, C., Yan, Q., Zhao, J. and Wang, J., Formulation of ultimate bearing capacity for strip foundations based on the Meyerhof theory and unsaturated soil mechanics. *Comput. Geotech.*, 2020, **126**, 103734; <https://doi.org/10.1016/j.compgeo.2020.103734>.

16. Jin, L., Zhang, H. and Feng, Q., Application of improved radial movement optimization for calculating the upper bound of ultimate bearing capacity of shallow foundation on unsaturated soil. *Comput. Geotech.*, 2019, **109**, 82–88; <https://doi.org/10.1016/j.compgeo.2019.01.016>.
17. Vo, T. and Russell, A. R., Bearing capacity of strip footings on unsaturated soils by the slip line theory. *Comput. Geotech.*, 2016, **74**, 122–131; <https://doi.org/10.1016/j.compgeo.2015.12.016>.
18. van Genuchten, M. Th., A closed-form equation predicting the hydraulic conductivity of unsaturated soils. *Soil Sci. Soc. Am. J.*, 1980, **44**(5), 892–898; <https://doi.org/10.2136/sssaj1980.0361599-5004400050002x>.
19. Oh, W. T. and Vanapalli, S. K., Modeling the stress versus settlement behavior of shallow foundations in unsaturated cohesive soils extending the modified total stress approach. *Soils Found.*, 2018, **58**(2), 382–397; <https://doi.org/10.1016/j.sandf.2018.02.008>.
20. Li, D. Q., Wang, L., Cao, Z. J. and Qi, X. H., Reliability analysis of unsaturated slope stability considering SWCC model selection and parameter uncertainties. *Eng. Geol.*, 2019, **260**, 105207; <https://doi.org/10.1016/j.enggeo.2019.105207>.
21. Hu, Y., Zhao, T., Wang, Y., Choi, C. and Ng, C. W. W., Direct simulation of two-dimensional isotropic or anisotropic random field from sparse measurement using Bayesian compressive sampling. *Stochast. Environ. Res. Risk Assess.*, 2019, **33**, 1477–1496; <https://doi.org/10.1007/s00477-019-01718-7>.
22. Shi, L., Yang, J. and Zhang, D., A stochastic approach to nonlinear unconfined flow subject to multiple random fields. *Stochast. Environ. Res. Risk Assess.*, 2009, **23**, 823–835; <https://doi.org/10.1007/s00477-008-0261-3>.
23. Lu, N., Godt, J. W. and Wu, D. T., A closed-form equation for effective stress in unsaturated soil. *Water Resour. Res.*, 2010, **46**(5), W05515; <https://doi.org/10.1029/2009WR008646>.
24. Bishop, A. W., The use of pore water coefficients in practice. *Geotechnique*, 1954, **4**, 148–152; <https://doi.org/10.1680/geot.1954.4.4.148>.
25. Wu, Y., Zhou, X., Gao, Y., Zhang, L. and Yang, J., Effect of soil variability on bearing capacity accounting for non-stationary characteristics of undrained shear strength. *Comput. Geotech.*, 2019, **110**, 199–210; <https://doi.org/10.1016/j.compgeo.2019.02.003>.
26. Chen, W. F., *Limit Analysis and Soil Plasticity*, Elsevier, 2013.
27. Zhou, J. and Qin, C., Finite element upper bound analysis of seismic slope stability considering pseudo-dynamic approach. *Comput. Geotech.*, 2020, **122**, 103530; <https://doi.org/10.1016/j.compgeo.2020.103530>.
28. Martin, C. M., The use of adaptive finite-element limit analysis to reveal slip-line fields. *Geotech. Lett.*, 2011, **1**(2), 23–29; <https://doi.org/10.1680/geolett.11.00018>.
29. Anand, A. and Sarkar, R., A probabilistic investigation on bearing capacity of unsaturated fly ash. *J. Hazard. Toxic Radioact. Waste*, 2020, **24**(4), 06020004; [https://doi.org/10.1061/\(ASCE\)HZ.2153-5515.0000547](https://doi.org/10.1061/(ASCE)HZ.2153-5515.0000547).
30. Terzaghi, K., *Theoretical Soil Mechanics*, Wiley, New York, USA, 1943.
31. Cho, S. E. and Park, H. C., Effect of spatial variability of cross-correlated soil properties on bearing capacity of strip footing. *Int. J. Num. Anal. Methods Geomech.*, 2010, **34**, 1–26; <https://doi.org/10.1002/nag.791>.
32. Griffiths, D. V. and Fenton, G. A., Bearing capacity of spatially random soil: the undrained clay Prandtl problem revisited. *Geotechnique*, 2001, **51**(4), 351–359; <https://doi.org/10.1680/geot.2001.51.4.351>.
33. Lu, N. and Likos, W. J., *Unsaturated Soil Mechanics*, Wiley, New York, USA, 2004.
34. Lee, I. K., White, W. and Ingles, O. G., *Geotechnical Engineering*, Pitman, London, UK, 1983.
35. Griffiths, D. V., Fenton, G. A. and Manoharan, N., Bearing capacity of rough rigid strip footing on cohesive soil: probabilistic study. *J. Geotech. Geoenviron. Eng.*, 2002, **128**, 743–755; [https://doi.org/10.1061/\(ASCE\)1090-0241\(2002\)128:9\(743\)](https://doi.org/10.1061/(ASCE)1090-0241(2002)128:9(743)).
36. Shu, S., Gao, Y., Wu, Y. and Ye, Z., Undrained bearing capacity of two strip footings on a spatially variable soil with linearly increasing mean strength. *Int. J. Geomech.*, 2021, **21**(2); [https://doi.org/10.1061/\(ASCE\)GM.1943-5622.0001904](https://doi.org/10.1061/(ASCE)GM.1943-5622.0001904).

ACKNOWLEDGEMENT. We thank the OptumG2 team for providing us the full academic license.

Received 30 July 2021; re-revised accepted 10 January 2022

doi: 10.18520/cs/v122/i5/542-556